dicated, although the degree of depletion is much less than that inferred from the Voyager result. Another argument in favor of an actual depletion of He is the large depletion of Ne observed by the mass spectrometer on the Galileo probe (*17*). A plausible explanation that deserves further exploration (*18*) is that Ne is soluble in the He-rich drops and is carried down by them.

REFERENCES AND NOTES

1. J. S. Lewis, *Sci. Am.* **230**, 51 (March 1974); M. Podolak and A. G. W. Cameron, *Icarus* **25**, 627 (1975).
2. B. J. Conrath, D. Gautier, R. A. Hanel, J. S. Hornstein, *Astrophys. J.* **282**, 807 (1984). Even though that paper deals predominantly with Saturn, it also contains the revised and most recent value for the He mass fraction in Jupiter's atmosphere as obtained from the Voyager experiments.
3. B. Conrath, D. Gautier, R. Hanel, G. Lindal, A. Marten, *J. Geophys. Res.* **92**, 15003 (1987).
4. W. B. Hubbard, in *Origin and Evolution of Planetary and Satellite Atmospheres*, S. K. Atreya, J. B. Pollack, M. S. Matthews, Eds. (Univ. of Arizona Press, Tucson, AZ, 1989), pp. 539–563.
5. M. Stix, *The Sun* (Springer Verlag, Berlin, Germany, 1989).
6. U. von Zahn and D. M. Hunten, *Space Sci. Rev.* **60**, 263 (1992).
7. F. A. Jenkins and H. E. White, *Fundamentals of Optics* (McGraw-Hill, New York, ed. 4, 1976). The light source is a light-emitting diode operating at a wavelength (λ) of 900 nm. An interference filter aids in producing near-monochromatic light. Two plane-parallel glass plates (Jamin plates) produce and recombine two parallel and coherent light beams. The SGC and RGC house the sample gas and a reference gas, respectively. Each has an effective length of 200 mm. Additional optical elements produce a well-defined pattern of consecutive equidistant bright and dark interference fringes at a linear array of nine photodetectors (PDA). The reference gas consists of a mixture of Ar and Ne having the same refractive index as a mixture of 10.95% He and 89.05% H_2. The reference gas was carried along to Jupiter within the instrument.
8. To write down the aggregate equation for calculating q_{He} we introduce the refractivities $R = 10^6\,(n - 1)$. Also, all parameters with the superscript 0 are taken at standard temperature and pressure. Other symbols are defined in the text before Eq. 2. One then obtains
$$q_{He} = + \frac{R^0_{H_2} Z^0_{H_2} - R^0_r Z^0_r}{R^0_{H_2} Z^0_{H_2} - R^0_{He} Z^0_{He}} + \frac{1}{R^0_{H_2} Z^0_{H_2} - R^0_{He} Z^0_{He}} \left(\frac{10^6\,\lambda P^0}{LT^0}\right)\left(\frac{F^e - F^i}{P^e_s/T^e_s Z^e_s - P^i_s/T^i_s Z^i_s}\right) + \frac{R^0_r Z^0_r}{R^0_{H_2} Z^0_{H_2} - R^0_{He} Z^0_{He}}\left[1 - \frac{P^e_r/T^e_r Z^e_r - P^i_r/T^i_r Z^i_r}{P^e_s/T^e_s Z^e_s - P^i_s/T^i_s Z^i_s}\right] \tag{3}$$
$$- (0.03301) q_{He,uncorr.} - 0.02189 + (7.933 \times 10^{-5}) T_{absorber}$$
9. For a binary gas mixture of H_2 and He, the mass fraction Y is obtained from the He mole fraction q_{He} by
$$Y = \frac{q_{He}}{m_H \frac{2}{m_{He}} + \left(1 - m_H \frac{2}{m_{He}}\right) q_{He}} \tag{4}$$
with m_{H2} and m_{He} being the masses of a H_2 molecule and a He atom, respectively (m_{H2}/m_{He} = 0.5036).
10. E. Anders and N. Grevesse, *Geochim. Cosmochim. Acta* **53**, 197 (1989).
11. A. G. Kosovichev *et al.*, *Mon. Not. R. Astron. Sci.* **259**, 536 (1992); F. Perez-Hernandez and J. Christensen-Dalsgaard, *ibid.* **269**, 475 (1994); S. Basu and H. M. Antia, in *Helioseismology*, J. T. Hoeksma, V. Domingo, B. Fleck, B. Battrick, Eds. [European Space Agency (ESA) special publication 376, ESA Publications Division, Noordwijk, Netherlands, 1995), p. 35.
12. J. N. Bahcall and M. H. Pinsonneault, *Rev. Mod. Phys.* **64**, 885 (1992).
13. C. R. Proffitt, *Astrophys. J.* **425**, 849 (1994). One of these models has a protosolar y = 0.280 and an atmospheric y = 0.251, and at the center y = 0.649 from hydrogen burning.
14. K. A. Olive and G. Steigman, *Astrophys. J. Suppl.* **97**, 49 (1995).
15. R. Smoluchowski, *Nature* **215**, 691 (1967); E. E. Salpeter, *Astrophys. J. Lett.* **181**, L183 (1973); D. J. Stevenson and E. E. Salpeter, *Astrophys. J. Supp.* **35**, 221 (1977); *ibid.*, p. 239.
16. G. Chabrier, D. Saumon, W. B. Hubbard, J. I. Lunine, *Astrophys. J.* **391**, 817 (1992); T. Guillot, G. Chabrier, P. Morel, D. Gautier, *Icarus* **112**, 354 (1994).
17. H. B. Niemann *et al.*, *Science* **272**, 846 (1996).
18. M. S. Roulston and D. J. Stevenson, *Eos* (fall suppl.) **76**, 343 (1995).

19. We thank our many colleagues and students for their diligent and untiring efforts on behalf of the HAD experiment. Over the years, H. J. Hoffmann contributed heavily to the instrument development effort; W. Mett was responsible for radiation hardening of instrument subsystems and W. Schulte for laboratory simulations of the instrument descent into the jovian atmosphere; H. Schütze performed the calibration and environmental tests of the three units of HAD instruments; H. Schütze and G. Lehmacher supported integration of the instrument into the spacecraft and systems tests; K. Pelka and G. Lehmacher assisted us through software development; and W. B. Hubbard was most helpful with advice on the high-pressure behavior of H-He mixtures. The interferometer part of the HAD instrument was developed by C. Zeiss, Oberkochen, Germany, and the other portion of the HAD was developed by Messerschmitt-Bölkow-Blohm, Ottobrunn, Germany. Supported by grants 50QJ90060 and 50QJ9501 of DARA GmbH; the German Space Agency, Bonn; and contract 958696 from the Jet Propulsion Laboratory.

5 March 1996; accepted 17 April 1996

Solar and Thermal Radiation in Jupiter's Atmosphere: Initial Results of the Galileo Probe Net Flux Radiometer

L. A. Sromovsky,* F. A. Best, A. D. Collard, P. M. Fry, H. E. Revercomb, R. S. Freedman, G. S. Orton, J. L. Hayden, M. G. Tomasko, M. T. Lemmon

The Galileo probe net flux radiometer measured radiation within Jupiter's atmosphere over the 125-kilometer altitude range between pressures of 0.44 bar and 14 bars. Evidence for the expected ammonia cloud was seen in solar and thermal channels down to 0.5 to 0.6 bar. Between 0.6 and 10 bars large thermal fluxes imply very low gaseous opacities and provide no evidence for a deep water cloud. Near 8 bars the water vapor abundance appears to be about 10 percent of what would be expected for a solar abundance of oxygen. Below 8 bars, measurements suggest an increasing water abundance with depth or a deep cloud layer. Ammonia appears to follow a significantly subsaturated profile above 3 bars. Unexpectedly high absorption of sunlight was found at wavelengths greater than 600 nanometers.

As the Galileo probe descended into Jupiter's atmosphere, the net flux radiometer (NFR) measured net solar and thermal radiation fluxes to determine where and how the atmosphere was being heated and cooled by radiation. The net flux, which is the difference between upward and downward fluxes, is useful because its divergence is equal to the radiative power per unit volume absorbed by the atmosphere. Thus, the vertical derivative of the NFR measurements defines the vertical distribution of radiative heating and cooling, which leads to buoyancy differences that power atmospheric circulations. NFR data also contain information about the opacity structure of Jupiter's atmosphere, which helps determine the distribution of particles and gases through which radiative transfer occurs. The relation between opacity sources and the radiative energy exchanges is important to understand in applying these very local measurements at the probe entry site, where exceptional atmospheric clarity is implied by ground-based observations (*1*), to other regions of Jupiter having different cloud structures and absorbing gas profiles.

The NFR (*2*) used an optical head that extended through the probe wall to obtain views of the jovian atmosphere. It sampled upward and downward fluxes with 40° (full angle) conical fields of view centered at directions ±45° from horizontal, avoiding most of the direct solar beam, but admitting a small fraction near the limits of its angular response. The NFR made measurements in five parallel spectral channels (Fig. 1). Two

L. A. Sromovsky, F. A. Best, A. D. Collard, P. M. Fry, H. E. Revercomb, University of Wisconsin, Madison, WI 53706, USA.
R. S. Freedman, Ames Research Center, Moffett Field, CA 94035, USA.
G. S. Orton, Jet Propulsion Laboratory, Pasadena, CA 91109, USA.
J. L. Hayden, Lockheed Martin Astronautics, Denver, CO 80201, USA.
M. G. Tomasko and M. T. Lemmon, University of Arizona, Tucson, AZ 85721, USA.

*To whom correspondence should be addressed. E-mail: lsromovsky@ssec.wisc.edu

solar channels provided a complete integration of all solar wavelengths (channel B, 0.3 to 3.5 μm) and a red-weighted subset in which methane absorption is most significant (channel E, 0.6 to 3.5 μm). Channel A (3 to 500 μm) measured sources and sinks of Jupiter's thermal radiation as a whole; channel C (3.5 to 5.8 μm) sampled the narrow-band 5-μm window in Jupiter's atmosphere where gaseous absorption is relatively low; and channel D (14 to 200 μm) sampled the hydrogen-dominated long-wavelength region of the thermal spectrum. All the thermal channels are sensitive to NH_3 and H_2O opacity to varying degrees, and channels A and C are also sensitive to cloud opacity. Channel F is a blind channel that measured nonradiative detector perturbations needed to correct for similar perturbations in the other channels.

The NFR began operating at an atmospheric pressure of ~0.415 bar, confirmed the heat shield jettison at ~0.44 bar, and operated until the mission terminated at a pressure of ~22 bars. As a result of unexpected temperature extremes inside the probe (3), the NFR detector package suffered a premature loss of responsivity such that useful radiation flux measurements do not extend deeper than about 14 bars, and results between 11 and 14 bars require responsivity corrections to be extrapolated beyond the range measured in prelaunch calibrations (4). Diagnostic measurements during descent confirm that in other respects the NFR operated as expected. An on-board heated blackbody reference provided useful calibration checks of thermal channels A and D between 2 and 13 bars, and of channel C between 6 and 13 bars. The agreement between expected and measured reference fluxes shows that the window common to all channels was not significantly contaminated, that the optical head was chopping properly (also confirmed by position sensors), and that the radiometric channels responded to radiation at about the level expected from prelaunch calibrations and in-flight tests.

During the measurement of atmospheric fluxes, the NFR detectors all respond to the sum of two thermal signals: One signal is the desired temperature modulation produced by a 2 Hz–modulated radiation input absorbed at the detector surface after it has passed through the optical system as the NFR chops between upward and downward views of the atmosphere, and the other signal is an extraneous undesired temperature modulation produced by slight variations in the bulk heating or cooling of the detector package (5). Although the blind channel (F) provides a measure of the extraneous signal, it cannot simply be subtracted from the signals of the other channels because the extraneous signal has a different size for each detector, presumably because of the temperature gradients within the detector package (6). Thus, additional constraints are needed to derive corrected flux profiles. From an examination of raw detector signals at the highest pressures, where channel D fluxes are certain to approach zero because of the dominance of increasing H_2 opacity, and where solar channel fluxes go to zero because of sunset, it appears that the vertical variations of the extraneous signals in these channels are in reasonable agreement with the channel F profile. It is also apparent that the channel F signature appears in the channel C profile at low pressures where its fluxes are expected to be small. On the basis of these comparisons, we used the altitude dependence of channel F to define the relative altitude dependence of the extraneous signals in the other channels. We subtracted from those channels an offset equal to the channel F waveform multiplied by a constant that made the corrected fluxes (Fig. 2) consistent with simple physical constraints (7).

Where the correction procedure has no influence—that is, near 0.45 and 2.3 bars, where channel F is zero—the flux measurements remain physically reasonable: Solar fluxes are negative, with channel B larger in absolute value than channel E, and thermal fluxes are positive, with reasonable ratios between channels (Fig. 2). The uncertainties that should be attached to these profiles arise from measurement noise and correction errors, both varying with altitude. The measurement noise is indicated by the scatter among points at adjacent altitudes. The correction errors are thought to be proportional to the channel F signal, and at 10 bars these errors are about equal to the scatter in the corrected observations at that level. Between 0.8 and 1.4 bars there is a region of partially correlated variation that we believe is due to thermal or other nonradiative perturbations.

Whereas the thermal channels indicate radiative cooling throughout most of the atmosphere, the broadband thermal channel above 0.6 bar indicates a radiative heating comparable with what would be expected from an NH_3 cloud of large particles (arbitrarily chosen as 100 μm in radius) with an optical depth of about 2 at 0.5 μm. Evidence for this cloud can also be seen in the correlated variations in the two solar channels

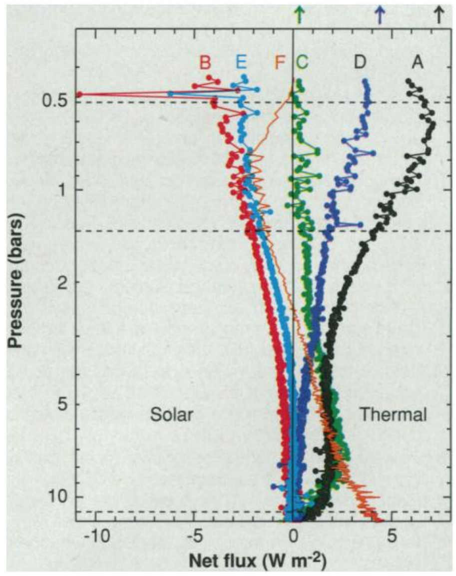

Fig. 2. Corrected NFR net flux observations (7). The blind channel (F) profile (orange line) is shown in flux units for comparison with channel A (different conversions would be needed to compare F with other channels). Because the sign of the net flux is chosen as positive upward, all thermal channels are positive and the two solar channels are negative. Where a net flux profile tilts to the left (with increasing height), radiative heating is occurring, whereas a tilt to the right indicates radiative cooling. The pressure scale is derived from the Jet Propulsion Laboratory–predicted descent profile with a time offset adjusted to match the predicted pressures to those of the atmospheric structure instrument P1 sensor (17). The arrows show the top-of-atmosphere thermal channel fluxes computed with the NEB hot spot model (13). The horizontal dashed line at 0.52 bars marks the base of the NH_3 cloud in that model, whereas the line at 1.36 bars marks the base of the only well-defined cloud detected by the nephelometer (10). The dashed line at 11 bars indicates where NFR detector temperatures exceed the range used in ground-based calibrations.

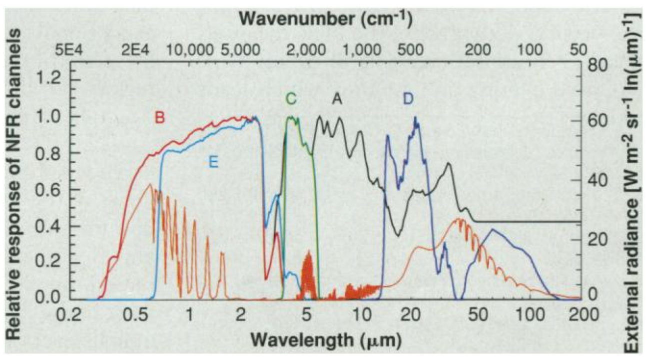

Fig. 1. Relative spectral responses of NFR spectral channels A to E. For comparison, top-of-atmosphere nadir-viewing external reflected solar and emitted thermal spectra of Jupiter are shown for Carlson *et al.* (13) North Equatorial Belt (NEB) hot spot cloud conditions (orange line). The NFR response at wavelengths greater than 50 μm is uncertain and still under investigation. Within the atmosphere the net radiation spectrum is considerably altered by increasing temperatures and local opacity sources.

between deployment and 0.5 to 0.6 bar. The nearly complete absence of these variations in the thermal channels confirms that the variation is due to a solar spectral source rather than an extraneous noise source. These variations cannot be due to true net flux variations because they would indicate regions of radiative cooling at solar wavelengths. Instead, they are consistent with variations expected from direct solar beam input at the edges of the NFR field of view, varying as a result of the probe spin during descent (*8*). From the way the spin-induced variations decay with depth, we estimate that there is an optical depth of about 1.5 to 2 of cloud material above the 0.5- to 0.6-bar level, roughly consistent with what is required to reproduce the thermal heating signature measured by channel A. This cloud is presumably the NH_3 ice cloud expected from ground-based and Voyager observations to occupy the pressure range from 0.25 bar to 0.6 to 0.7 bar at low to mid latitudes, including regions of hot spots (*9*). The low levels of particulate scattering measured by the nephelometer in this region (*10*) suggest a heterogeneous cloud structure (*11*). An alternate explanation that seems less plausible is that the particles are of an unusual size or shape that would inhibit their detection by the nephelometer.

The nephelometer detected the base of a relatively well-defined cloud of optical depth tentatively estimated as 2.6 (*10*) near the 1.36-bar level (using the pressure scale in Fig. 2). There does seem to be an indication of a cloud at that level in NFR channel C, where net fluxes above the cloud are ~50% less than those below the cloud, which is about the attenuation expected for an NH_4SH cloud of unit optical depth. However, the magnitude of the observed effect is quite uncertain because of increased noise above the cloud base and uncertainty in the channel F correction factor. In channel A, a relatively strong vertical gradient throughout the cloud layer impedes detection of a subtle cloud signature. However, an NH_4SH cloud of optical depth greater than unity should produce a clear signature that is not seen in the observations. The same cloud should not produce significant perturbations of the solar profiles or of the channel D thermal profile, and none are seen. Although the solar and thermal channel profiles do not provide strong evidence for a cloud base at 1.36 bars, they are not clearly inconsistent with the cloud detected by the nephelometer (*10*), given its currently uncertain composition.

The decline of solar channel fluxes with depth arises from atmospheric absorption and from the setting of the sun during descent. The solar zenith angle for NFR measurements was approximately 67° at deployment and increased to 90° as the probe reached about the 15-bar level. The decline of the channel E signal to zero at the 5-bar level, accompanied by the consistent parallel decline in channel B, seems to require a nearly complete absorption of light in the red part of the spectrum (wavelength > 600 nm), a result inconsistent with expectations. Although methane is a major absorber within the channel E bandpass, our current understanding of its abundance and absorbing properties (*12*) leads to a substantially slower predicted decline.

The broadband thermal channel (A) indicates a weak heating in the region between 3 and 8 bars. This is probably not an indication of the presence of particles, because model calculations show this effect with only expected gas opacity included. Notably absent is any signature of increased cloud-top cooling or cloud-base heating that might provide evidence for an opaque water cloud in the 5- to 6-bar region. However, there is a relatively strong cooling signature seen between 9 and 11 bars, implying an increase of opacity with depth below 9 bars. Either a strongly increasing water vapor mixing ratio or a layer of particles might be responsible.

Using the North Equatorial Belt hot spot model of Carlson *et al.* (*13*), which uses deep mixing ratios of two times the solar abundance for water, three times the solar abundance for methane, and 2.5 times the solar abundance for ammonia (*14*), we calculated model flux levels at the top of the atmosphere (Fig. 2) that are in rough agreement with the highest altitude NFR measurements; what differences are seen might be expected from opacity sources above the first NFR measurements. However, within the atmosphere this model leads to much smaller fluxes than those observed by the NFR (note the channel A comparison in Fig. 3). To match measured NFR flux levels within the atmosphere requires a set of minor gas mixing ratio profiles and cloud amounts that lead to very low atmospheric opacity. The nonunique fit to the channel A profile (Fig. 3) provides one example that uses the following gas distribution: Ammonia was set to a constant solar abundance mixing ratio deeper than 3 bars, but significantly subsaturated above; water was set to 20% of solar abundance deeper than 10 bars, decreasing to 10% of solar abundance between 10 and 8 bars, remaining at 10% to 6 bars, and decreasing by a factor of 10 from 6 to 3 bars; and the NH_3 cloud optical depth was set to 2 at 0.5 μm and the particle radius to 100 μm (a mid-level NH_4SH cloud was not included). To illustrate the sensitivity of these profiles to water vapor abundance, we used two additional curves corresponding to one-half and two times the mixing ratios used in the fitted model (Fig. 3). The sensitivity of the NFR channel A models to deep NH_3 variations is sufficiently low that current uncertainties in the well-mixed NH_3 abundance (*15*) produce model variations smaller than the scatter in the NFR observations.

The NFR channel A observations are most consistent with a water vapor abundance of 0.1 to 0.2 times the solar abundance in the 6- to 12-bar range, the larger value agreeing with the neutral mass spectrometer results (*16*). However, the increased opacity between 8 and 12 bars could also be modeled by using a cloud layer instead of a layer of increasing water vapor abundance, in which case the water vapor mixing ratio could be a constant 10% of solar abundance below ~6 bars. Between 3 and 6 bars, some combination of subsaturation of water and ammonia is required to match the NFR observations. At lower pressures, the NFR observations are insensitive to water, but they do seem to require ammonia to be significantly more subsatu-

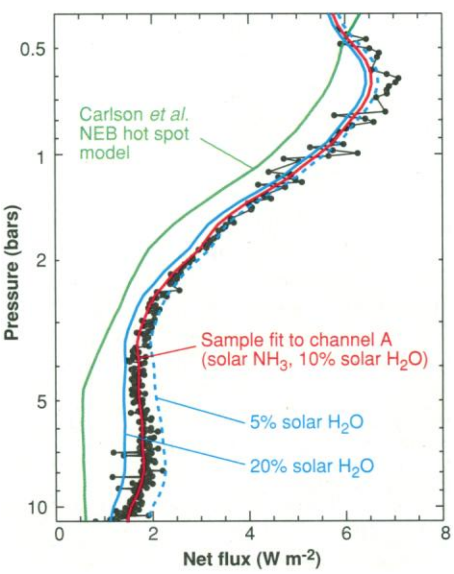

Fig. 3. NFR broadband thermal flux measurements (channel A) compared with radiation transfer model calculations under various assumptions about gas mixing ratios. The NFR observations are plotted as filled circles. Measurement and correction errors are of the order of the scatter in points at nearby altitudes. The model (red) that fits the channel A observations uses a vertical profile of water vapor (described in the text) in which the abundance between 6 and 8 bars is 10% of solar abundance (*14*). Calculated flux profiles are also shown for models in which the water abundances are doubled and halved (solid and dashed blue curves, respectively). The NEB hot spot model (*13*) (green curve) uses a deep water vapor mixing ratio that is twice the solar abundance.

rated than previously estimated. For example, the ammonia profile of Carlson *et al.* (*13*) decreases by a factor of 10 from 2 bars to 1 bar, whereas our fitted profile decreases by more than a factor of 20 between 3 bars and 1 bar, and decreases by another factor of 4 between 1 and 0.5 bars, where their profile is constant. It remains to be determined whether we can find an opacity structure that is not only consistent with NFR observations but also satisfies other constraints derived from recent ground-based or past Voyager observations of hot spots.

REFERENCES AND NOTES

1. G. S. Orton *et al.*, *Science* **272**, 839 (1996).
2. L. A. Sromovsky, J. Hayden, F. A. Best, H. E. Revercomb, *Space Sci. Rev.* **60**, 233 (1992).
3. R. E. Young, M. A. Smith, C. K. Sobeck, *Science* **272**, 837 (1996).
4. Prelaunch calibrations are described in (*2*) and in more detail by L. A. Sromovsky and P. M. Fry [in *Proceedings of The Fourth Infrared Sensor Calibration Symposium*, 9 to 12 May 1994, Space Dynamics Laboratory, Utah State Univ., Logan, UT (1994).
5. The detector heating and cooling is modulated by the rotation of the optics (including the detector package) between upward and downward views, exposing the detector package to convective transfer rates that vary with orientation at the chopping frequency, and thus can produce a very small temperature modulation in the pyroelectric detectors at the same frequency as the desired temperature modulations produced by the chopped radiation signal.
6. Detector-to-detector variations are currently not well understood and are the subject of laboratory tests of the spare instrument.
7. For each solar channel, we multiplied the blind channel correction by a factor that produced net fluxes approaching zero toward sunset (about 15 bars). For channel D, we required that the net flux at 10 bars be in the range of 0 to 0.3 W m^{-2}, the upper bound being the maximum possible flux computed for a model in which only hydrogen absorption is present. For channel C we used a model-independent requirement that the measured fluxes be positive at all altitudes, and we obtained slightly tighter constraints by also requiring that (when averaged over noise) channel C fluxes decrease with height above the 3-bar level. The correction of the broadband thermal channel (A) was guided by model calculations showing that net fluxes in the 3- to 10-bar region were dominated by the 5-μm fluxes, with most of the remainder coming from the hydrogen-dominated region sampled by channel D. But because of differences in relative spectral response functions, the model results indicate that channel C and channel A should be about equal in the 8- to 10-bar region. Thus, we selected the channel A correction factor to minimize its average difference with channel C deeper than about 8 bars. We determined the following extraneous response correction factors: channel A, 1.4 $\pm$ 0.1; channel B, 0.75 $\pm$ 0.1; channel C, 4.0 $\pm$ 0.2; channel D, 2.1 $\pm$ 0.05; and channel E, 1.3 $\pm$ 0.05. These are the factors by which the channel F detector–level output needs to be multiplied before being subtracted from the other channels to correct for their extraneous response signals. The uncertainties for channels B, C, D, and E arise mainly from noise in the profiles in regions where the constraints are applied. The relatively large correction required for channel C is not understood and suggests that a very localized heat transfer near the detector package itself is needed to introduce such a difference in temperature variation amplitudes.
8. The probe spin rate appears to be a relatively constant 33.5 (+2.6/−2.4) rpm down to at least the 1-bar level (L. J. Lanzerotti and K. Rinnaert, personal communication). The mean azimuthal position of a 6-s sampling interval would thus change ~126° (+93°/−80°) between samples, implying that a sample facing the sun would be surrounded by samples facing away from the sun, leading to a modulation of amplitude that depends on the initial azimuth.
9. R. A. West, D. F. Strobel, M. G. Tomasko, *Icarus* **65**, 161 (1986).
10. B. Ragent, D. S. Colburn, P. Avrin, K. A. Rages, *Science* **272**, 855 (1996).
11. If the NH_3 cloud layer were composed of broken clouds above the probe, or if the probe were in a clear region within the cloud layer, the heating in channel A and the effects of direct solar beam attenuation in channels B and E could still be seen by the NFR, which observes radiation from distances of many kilometers. On the other hand, the nephelometer, which samples only the immediate vicinity of the probe, would see nothing.
12. L. P. Giver, M. G. Tomasko, D. Kerola, D. C. Benner, *Bull. Am. Astron. Soc.* **21**, 947 (1989); E. Karkoschka, *Icarus* **111**, 174 (1994).
13. B. E. Carlson, A. C. Lacis, W. B. Rossow, *J. Geophys. Res.* **98**, 5251 (1993).
14. Solar mixing ratios, expressed as number densities relative to H_2, are taken to be 1.7×10^{-3} for H_2O, 7.2×10^{-4} for CH_4, and 2.2×10^{-4} for NH_3, following E. Anders and N. Grevesse [*Geochim. Cosmochim. Acta* **53**, 197 (1989)].
15. The current best estimate for the jovian deep NH_3 abundance is 1.3 $\pm$ (0.1 to 0.2) times the solar abundance, on the basis of analysis of microwave observations by I. De Pater and D. L. Mitchell [*J. Geophys. Res. Planets* **98**, 5471 (1993)].
16. H. B. Niemann *et al.*, *Science* **272**, 846 (1996).
17. A. Seiff *et al.*, *Science* **272**, 844 (1996).

18. Special recognition is due to R. W. Boese, the original NFR principal investigator from Ames Research Center (ARC), who died in 1985, and J. Pollack, a key NFR co-investigator, who died in June 1994. We thank R. Twarowski and B. Chin from ARC for valuable project support; the following M. Marietta personnel involved in the NFR development: D. Shumaker, T. Knight, R. Amundsen, T. Hopkins, S. Shertz, and B. Cunningham; P. Smith and L. Doose from the University of Arizona, who supported the NFR calibration; D. Thielman, J. Vian, S. Ellington, J. Sitzman, and M. Dean, who provided support at the University of Wisconsin; the Galileo Project, and W. J. O'Neil in particular, for providing support and guidance; B. Carlson of the Goddard Institute for Space Studies for help in checking our radiative transfer model calculations; and an anonymous reviewer for helpful comments on the original draft. During the postlaunch period, the University of Wisconsin effort was supported by NASA grant NCC2-854.

4 March 1996; accepted 17 April 1996

Results of the Galileo Probe Nephelometer Experiment

Boris Ragent,* David S. Colburn, Philip Avrin, Kathy A. Rages

The nephelometer experiment carried on the Galileo probe was designed to measure the jovian cloud structure and its microphysical characteristics from entry down to atmospheric pressure levels greater than 10 bars. Before this mission there was no direct evidence for the existence of the clouds below the uppermost cloud layer, and only theoretical models derived from remote sensing observations were available for describing such clouds. Only one significant cloud structure with a base at about 1.55 bars was found along the probe descent trajectory below an ambient pressure of about 0.4 bar, although many indications of small densities of particle concentrations were noted during much of the descent.

The objective of the nephelometer experiment (*1*) aboard the Galileo probe (*2, 3*) is to explore the vertical structure and microphysical properties of the clouds and hazes of the jovian atmosphere. The instrument measured the scattering of an incident light beam from defined volumes in the atmosphere near the probe at five angles, four at forward scattering angles and one in a backscattering direction. An arm containing reflective mirror optics was successfully deployed shortly after the heat shield and aeroshell were removed. The instrument functioned and data were recorded from an altitude of about 20 km (~0.4 bar) above the 1-bar pressure reference altitude down to an altitude of about −140 km (~22 bars) (*4*). Data were obtained over the entire probe reporting period, but the instrument began to exhibit erratic behavior after about 40 min (~13 bars) of descent and began to fail, presumably because of the extreme operating conditions (*5*).

After the probe entered the atmosphere and decelerated, the nephelometer experiment was turned on about 13 s before the heat shield separated from the probe. About 2 s after heat shield separation, squibs freeing the nephelometer mirror arm were fired, commencing measurement of the ambient jovian atmosphere. Since the first measurements were affected by all these events, the first viable atmospheric data were obtained about 19.7 s after the instrument was turned on, corresponding to an ambient atmospheric pressure and temperature of ~0.4 bar and 129 K. Data were obtained for the next 57 min. However, because the instrument deteriorated in the hot internal probe environment near the end of descent, valid data may have been obtained only for the

B. Ragent and D. S. Colburn, San Jose State University Foundation, San Jose, CA 95172–0130, USA.

P. Avrin, Aerospace Corporation, Colorado Springs, CO 80912, USA.

K. A. Rages, Space Physics Research Institute, Sunnyvale, CA 94087–1315, USA.

*To whom correspondence should be addressed.